Journal of Power Sources 440 (2019) 227123

Contents lists available at ScienceDirect

Journal of Power Sources

journal homepage: www.elsevier.com/locate/jpowsour

Multilayer NiMn layered double hydroxide nanosheets covered porous Co_3O_4 nanowire arrays with hierarchical structure for high-performance supercapacitors

Weiguo Huang [a,1], Aitang Zhang [a,1], Xiaoru Li [a], Jinmi Tian [a], Lijun Yue [a], Liang Cui [b,**], Rongkun Zheng [b], Di Wei [b], Jingquan Liu [a,*]

[a] College of Material Science and Engineering, Institute for Graphene Applied Technology Innovation, Collaborative Innovation Centre for Marine Biomass Fibers, Materials and Textiles of Shandong Province, Qingdao University, Qingdao, 266071, Shandong, China
[b] College of Materials Science and Engineering, Linyi University, Linyi, 276400, Shandong, China

HIGHLIGHTS

- The porous Co_3O_4 nanowires provide more paths for ions diffusion.
- NiMn layered double hydroxide nanosheets provide large surface areas.
- Co_3O_4@NiMn-LDH/Ni electrode exhibits excellent supercapacitive properties.

GRAPHICAL ABSTRACT

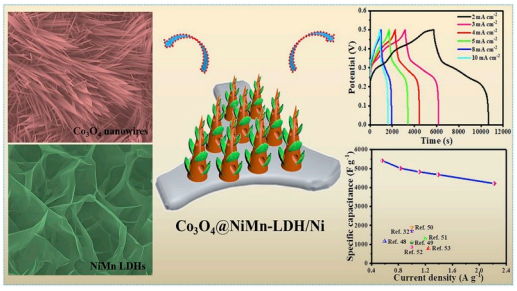

ARTICLE INFO

Keywords:
Porous Co_3O_4 nanowires
NiMn layered double hydroxides
Hierarchical nanostructure
Supercapacitor

ABSTRACT

The hierarchical nanostructure hybrids of porous Co_3O_4 nanowires coated NiMn layered double hydroxide nanosheets array on Ni foams (Co_3O_4@NiMn-LDH/Ni) are designed and prepared via the two-step hydrothermal reactions with a combination of annealing process. The Co_3O_4 nanowires can be utilized as backbone to grow the NiMn-layered double hydroxide (NiMn-LDH) nanosheets, which provide a large surface area and leading to the enhanced capacitive performance owing to the effective ion/electron diffusion rates. The areal capacitance of the as-prepared Co_3O_4@NiMn-LDH/Ni electrode reaches 19.7 F cm^{-2} (5419.7 F g^{-1}) at 2 mA cm^{-2} (0.56 A g^{-1}). Moreover, a high capacitance retention (93.25% of capacitance maintained after 6000 cycles) and a low internal resistance R_s (0.62 Ω) can be acquired. Additionally, an all-solid-state asymmetric supercapacitor (Co_3O_4@NiMn-LDH/Ni//AC ASC) based on the Co_3O_4@NiMn-LDH/Ni as positive electrode and activated carbon (AC) as negative electrode is successfully obtained. The Co_3O_4@NiMn-LDH/Ni//AC ASC shows a high energy density of 47.15 Wh kg^{-1} at 376 W kg^{-1}. Additionally, a LED can be lit up for 12 min when three ASCs are connected in series. Therefore, this novel Co_3O_4@NiMn-LDH/Ni with outstanding electrochemical performance should envision potential practical applications in high energy storage appliances.

* Corresponding author.
** Corresponding author.
E-mail addresses: clzkzy@163.com (L. Cui), jliu@qdu.edu.cn (J. Liu).
[1] Weiguo Huang and Aitang Zhang contributed equally to this work.

https://doi.org/10.1016/j.jpowsour.2019.227123
Received 13 June 2019; Received in revised form 2 August 2019; Accepted 5 September 2019
Available online 13 September 2019
0378-7753/

1. Introduction

High-efficient energy storage technology is crucial for fully usage of traditional fossil energy and renewable energy [1–4]. As an essential electrochemical energy storage device, supercapacitors (SCs) have obtained great attention due to their fast charge-discharge capability, high power density and remarkable recyclability [5–8]. Typically, the SCs can be classified into two sorts according to charge storage mechanisms: electrical double-layer capacitors (EDLCs) and pseudocapacitors. The charges are mainly adsorbed electrostatically on the boundary surface of electrode/electrolyte and a variety of materials like porous carbon nanosheets [9] and reduced graphene oxide [10] have been adopted as electrode materials for EDLCs. However, the carbon-based materials are usually suffer from a series of drawbacks such as the uncontrollable pore size and shape, insufficient electronic conductivity and long ion-diffusion distance (>5 μm), leading to compromised specific capacitance [11–14]. Compared with EDLCs, pseudocapacitors store energy by the faradaic redox reactions inside electrode material, whose electrodes are usually made of transition metal oxides/hydroxides and conducting polymers [15]. Recently, a variety of materials are designed to enhance the electrode properties, among which the transition metal oxides exhibited remarkable superiority owing to the high specific capacitance, good conductivity and large surface area [16].

Currently, various metal oxides like NiO, Fe_2O_3, WO_3 and Co_3O_4 are widely applied to electrode materials for supercapacitors owing to their high theoretical specific capacitances and abundant reserves. Among these metal oxide nanomaterials, cobalt oxide (Co_3O_4) has obtained extensive attention due to its special nanostructures, environmental friendliness and strong redox activity [17,18]. However, the single component of Co_3O_4 applied as supercapacitor electrode usually exhibited the poor electrode stability, low specific capacity (much lower than the theoretical value), inferior cyclic stability and so on, which significantly restricted its practical applications [19]. To overcome these defects, numerous efforts have been contributed to the ingenious design of nanocomposites with various structures and morphologies. It has been reported that the 3D hierarchical $CoWO_4/Co_3O_4$ composite arrayed on Ni foam by a facile microwave hydrothermal process and utilized as the electrode material of supercapacitors showed superior specific capacitance (1728 F g^{-1} at 2.7 mA cm^{-2} or 1 A g^{-1}), well rate capability and outstanding cycling stability (85.9% capacitance maintained after 3000 cycles) [20]. Moreover, a 2D Co_3O_4@$NiCo_2O_4$ nanowires composite arrayed on Ni foam via hydrothermal process and applied to the electrode material of supercapacitors revealed a specific capacitance of 9.12 F cm^{-2} at 2 mA cm^{-2}, remarkable cycling stability and superb energy density (75.6 Wh kg^{-1} at 1053 W kg^{-1}) [21]. Meanwhile, an effective strategy for preparing Co_3O_4-electrode materials with satisfactory electrochemical performance was utilized to construct the expected core/shell architecture. For example, the Co_3O_4@CoNi-LDH core/shell nanosheets were arrayed on Ni foam and used for electrode material of supercapacitor, which displayed large specific capacitance (2676.9 F g^{-1} at 0.5 A g^{-1}), excellent cycling stability and remarkable energy density (61.23 Wh kg^{-1} at 750 W kg^{-1}) [22]. Additionally, the Co_3O_4@NiO core/shell nanoarrays were obtained by a hydrothermal process and applied as the electrode material of supercapacitor, revealing a specific capacitance of up to 2018 mF cm^{-2} at 2 mA cm^{-2} and significant cycling stability (75.3% of capacitance maintained after 10 000 cycles) [23]. Notably, although plenty of efforts have been devoted to make a significant promotion in electrochemistry performance, essential studies to enhance the electrochemistry performances of Co_3O_4-based materials are still in great demand [24–26]. Recently, layered double hydroxides (LDH) have been widely explored as electrode materials for SCs, which exhibit excellent electrochemical performances owing to their tunable chemical composition, high redox reduction activity and large specific surface area [27,28]. Especially, the NiMn LDH nanosheet not only provides the large specific surface area but also exhibits the benign conductivity, which significantly increases the storage capacity. Therefore, combining Co_3O_4 with NiMn LDHs should be a well strategy to prepare the electrochemical active materials with desired performance.

In this work, we design and prepare the porous Co_3O_4 nanowires@NiMn layered double hydroxide nanosheets array on three-dimensional conductive Ni foam (Co_3O_4@NiMn-LDH/Ni) by the two-step hydrothermal reactions with a combination of annealing process. Subsequently, the obtained Co_3O_4@NiMn-LDH/Ni is directly applied to prepare binder-free electrodes which possess numerous virtues, such as larger quantity of active sites, higher utilization efficiency of active materials and faster ion/electron diffusion rates. The prepared Co_3O_4@NiMn-LDHs/Ni electrode shows an outstanding capacitance up to 19.7 F cm^{-2} (5419.7 F g^{-1}) at 2 mA cm^{-2} (0.56 A g^{-1}) in a three electrodes system, which are significantly superior to those of NiMn-LDH/Ni and Co_3O_4/Ni electrodes. A high capacitance retention (93.25% of capacitance maintained after 6000 cycles at 20 mA cm^{-2}) and a low internal resistance R_s (0.62 Ω) can be achieved. Furthermore, an asymmetric supercapacitor (Co_3O_4@NiMn-LDH/Ni//AC ASC) is prepared by applying the Co_3O_4@NiMn-LDH/Ni as the positive electrode and activated carbon (AC) as the negative electrode. The Co_3O_4@NiMn-LDH/Ni//AC ASC shows a high energy density of 47.15 Wh kg^{-1} at a power density of 376 W kg^{-1} and can be able to light up a LED indicator for 12 min by connecting three Co_3O_4@NiMn-LDH/Ni//AC ASCs in series, demonstrating the potential for practical applications.

2. Experimental section

2.1. Reagents

The Ni foam was purchased from Shanghai Zhongwei New Material Co., Ltd. Ethanol (AR) and hydrochloric acid (HCl) were supplied by Tianjin Fuyu Fine Chemical Co., Ltd. Cobalt nitrate hexahydrate (AR), hexamethylenetetramine (AR), ammonium fluoride (AR), nickel dichloride (AR), manganese (II) chloride tetrahydrate (AR), urea (AR), potassium hydroxide (AR), conductive acetylene black (AR) and arkema HSV900 PVDF binder (AR) were all purchased from Sinopharm Chemical Reagent Co., Ltd. All aqueous solutions were prepared using deionized water with a resistivity of 18.2 MΩ cm^{-1}.

2.2. Synthesis of porous Co_3O_4 nanowires array on Ni foam (Co_3O_4/Ni)

Before experiments, the Ni foam (1.0 × 1.0 cm^2) was ultrasonically cleaned with HCl solution (30 wt %), ethanol and deionized water for 30 min individually to remove the surface oxide layer and dried at 60 °C for 8 h in a drying oven. The porous Co_3O_4 nanowires were prepared by a hydrothermal reaction and calcination treatment. Typically, 1.164 g $Co(NO_3)_2{\cdot}6H_2O$, 1.200 g $CO(NH_2)_2$ and 0.296 g NH_4F were dissolved in 70 ml deionized water, the resulting mixture was stirred for 30 min to obtain a homogeneous pink solution. Subsequently, the pretreated Ni foam was immersed into the above mixed solution and reacted in a 100 mL teflon-lined stainless steel autoclave at 120 °C for 8 h. During the reaction, Co^{2+} can react with F^- to form intermediate product of $CoF_x^{(x-2)-}$. Meanwhile, urea can dissolve in water and provides both carbonate and hydroxyl anions. Subsequently, the CO_3^{2-} and OH^- react with $CoF_x^{(x-2)-}$ to generate cobalt hydroxide carbonate species ($Co_2(OH)_2CO_3{\cdot}nH_2O$) [29,30]. Moreover, NH_4F plays a significant part in the activation and self-assembly process for the construction of nanowires structure. The involved reactions can be illustrated by following equations [31]:

$$Co^{2+} + x\ F^- \rightarrow [CoF_x]^{(x-2)-}$$

$$CO(NH_2)_2 + H_2O \rightarrow 2\ NH_3 + CO_2$$

$$CO_2 + H_2O \rightarrow CO_3^{2-} + 2H^+$$

$$NH_3{\cdot}H_2O \rightarrow NH_4^+ + OH^-$$

$$2\ [CoF_x]^{(x-2)-} + 2\ OH^- + CO_3^{2-} + H_2O \rightarrow Co_2(OH)_2CO_3{\cdot}nH_2O + 2x\ F^-$$

Then, the resulting product was washed with ethanol and deionized several times and dried at 80 °C for 6 h in a vacuum drying oven. Finally, the dried product was calcined at 400 °C under air atmosphere for 3 h to obtain porous Co_3O_4 nanowire arrays. The $Co_2(OH)_2CO_3{\cdot}nH_2O$ arrays were transferred into Co_3O_4 nanowires arrays via the dehydration process of $Co_2(OH)_2CO_3{\cdot}nH_2O$. The involved reactions can be illustrated by the equation below (the heating process is marked by "Δ") [32]:

$$3Co_2(OH)_2CO_3{\cdot}nH_2O + O_2 \xrightarrow{\Delta} 2Co_3O_4 + 3CO_2 + 3(n+1)H_2O$$

2.3. Fabrication of porous Co_3O_4 nanowires coated NiMn layered double hydroxide nanosheets array on Ni foam (Co_3O_4@NiMn-LDH/Ni)

0.713 g $NiCl_2{\cdot}6H_2O$, 0.198 g $MnCl_2{\cdot}4H_2O$ and 0.700 g hexamethylenetetramine (HMT) were dissolved in 40 mL deionized water, the resulting mixture was stirred for 30 min to obtain a homogeneous solution. Then the as-obtained porous Co_3O_4/Ni was immersed into the mix solution and reacted in a 100 mL Teflon-lined stainless steel autoclave at 90 °C for 6 h. During the reaction, HMT can act as hydrolysis agent to alkalize aqueous solution and generate OH^-, then the Ni^{2+} and Mn^{2+} can react with OH^- to generate $(Ni_{1-x}Mn_x)(OH)_2$ nanosheets under an alkaline environment. Meanwhile, HMT plays a significant role in facilitating the formation of NiMn-LDHs with high crystallinity at a moderate temperature [33]. The involved reactions can be illustrated by the following equations [34]:

$$(CH_2)_6N_4 + 10H_2O \rightarrow 6\ HCHO + 4\ NH_4^+ + 4\ OH^-$$

$$(1\text{-}x)\ Ni^{2+} + x\ Mn^{2+} + 2\ OH^- \rightarrow (Ni_{1-x}Mn_x)(OH)_2$$

After cooled naturally, the Co_3O_4@NiMn-LDH/Ni was washed with ethanol and deionized water for several times and then dried at 60 °C for 8 h in a vacuum drying oven. For comparison, the NiMn layered double hydroxide directly arrayed on Ni foam (NiMn-LDH/Ni) was prepared at the same condition. The total mass loading of Co_3O_4@NiMn LDH arrays grown on the Ni foam was calculated to be 3.6 mg cm^{-2}.

2.4. Characterizations

A JEOL JSM-6700F scanning electron microscope (SEM) with an accelerating voltage of 5 kV was utilized to verify the morphology of samples. Transmission electron microscopy (TEM), high resolution transmission electron microscopy (HRTEM), energy dispersive X-ray spectroscopy (EDS) and element mapping images were performed on a JEOL2011 microscope operated at an acceleration voltage of 200 kV. The chemical structures of the materials were studied by X-ray photoelectron spectroscopy (XPS), a Kratos Axis Ultra DLD spectrometer employing a monochromated Al Ka X-ray source (h = 1486.7 eV). Moreover, the crystallographic structures of the materials were analyzed by a powder XRD system (DX-2700, λ = 0.15406 nm).

2.5. Fabrication of electrodes and electrochemical measurements

All the electrochemical measurements were measured on an electrochemical workstation (CHI 760E) at ambient temperature. Electrochemical performances of the samples were carried out in a three-electrode system with a platinum tablet as counter electrode and the Hg/HgO as reference electrode, respectively. In addition, the as-prepared Co_3O_4@NiMn-LDH/Ni ($1.0 \times 1.0\ cm^2$) was served as the working electrode and 6 M KOH aqueous solution as the electrolyte. Cyclic voltammetry (CV) tests were carried out at different scan rates of 10, 20, 30, 50 and 100 mV s^{-1}, respectively. Galvanostatic charge/discharge (GCD) curves were carried out at different current densities of 2, 3, 4, 5, 8 and 10 mA cm^{-2}, respectively. Moreover, electrochemical impedance spectroscopy (EIS) was carried out in the frequency response range from 100 kHz to 0.1 Hz with an open circuit potential a 5 mV AC perturbation. The specific capacitance of the electrodes was calculated by the following equation (1) [35]:

$$C_A = \frac{I\int Vdt}{sV^2} \quad (1)$$

where I (A) represents the discharge current, Δt (s) represents the discharge time, ΔV (V) represents the potential window, and s (cm^2) represents the effective area of electrode, respectively.

2.6. Fabrication and electrochemical measurements of asymmetric supercapacitor (ASC)

To prepare an active carbon (AC) electrode, active carbon, acetylene black and polyvinylidene fluoride (PVDF) were dissolved in ethanol with a mass ratio at 8 : 1: 1 to obtain a suspension mixture. Acetylene black and PVDF were utilized as a conductive agent and binder, respectively. Then, the obtained mixture was placed in a vacuum drying oven for drying treatment at 60 °C for 6 h. Lastly, the mixture was placed onto two nickel foams, followed by the pressing under 15 MPa for 5 s. The ASC device was prepared by applying Co_3O_4@NiMn-LDH/Ni ($1.0 \times 2.0\ cm^2$) as the positive electrode and AC as negative electrode, respectively, while 6 M KOH performed as the electrolyte. In order to obtain an all-solid-state ASC with excellent electrochemical performances, the relationship ($q^+ = q^-$) of charge balance among the two electrodes should be required. q represents the stored charge of the electrode, which can be calculated by the equation (2):

$$q = C \times m \times \Delta V \quad (2)$$

where C (F g^{-1}) represents the specific capacitance of the electrode, m (g) represents the mass of the active material and ΔV (V) represents the potential window. According to equation (2), the ideal mass ratio of electroactive material on the positive to that on negative electrodes in an all-solid-state ASC (m^+/m^-) can be calculated by the equation (3):

$$m^+ / m^- = C^-\Delta V^- / C^+\Delta V^+ \quad (3)$$

where C^+ (F g^{-1}) and C^- (F g^{-1}) represent the specific capacitance of Co_3O_4@NiMn-LDH/Ni and AC electrodes, respectively. ΔV^+ (V) and ΔV^- (V) represent the voltage range of Co_3O_4@NiMn-LDH/Ni and AC electrodes, respectively. The specific capacitance (C_s) of the ASC was calculated by the equation (4):

$$C_s = \frac{I\Delta t}{m\Delta V} \quad (4)$$

where I (A) represents the discharge current, Δt (s) represents the discharge time, ΔV (V) represents the potential window, and m (g) represents the total mass of active materials on both electrodes. The coulombic efficiency (η), the energy density E (Wh kg^{-1}) and power density P (W kg^{-1}) of ASC were calculated by the equations (5)–(7) [20,36]:

$$\eta = \frac{\Delta t_d}{\Delta t_c} \quad (5)$$

$$E = \frac{1}{2}C_s\Delta V^2 \quad (6)$$

$$P = \frac{E}{\Delta t} \quad (7)$$

where Δt_c represents the charging time, Δt_d represents the discharging time.

3. Results and discussion

The stepwise preparation of Co_3O_4@NiMn-LDH arrays grown on Ni foam (Co_3O_4@NiMn-LDH/Ni) is schematically illustrated in Fig. 1a. The Co_3O_4@NiMn-LDH/Ni was designed and prepared by the two-step hydrothermal reactions with a combination of annealing process. Firstly, the fascicular and spinous $Co_2(OH)_2CO_3$ arrays were anchored on Ni foam via a hydrothermal synthesis treatment (Step I). Secondly, the porous Co_3O_4 nanowires arrays were then obtained through the calcination process in an air atmosphere under 400 °C (Step II). Finally, the NiMn-LDH nanosheets were generated on the pre-prepared porous Co_3O_4 nanowires by the hydrothermal synthesis process under 90 °C (Step III). The microstructures of as-obtained samples were firstly investigated by scanning electron microscopy (SEM). The corresponding photographs of $Co_2(OH)_2CO_3$ precursor/Ni, Co_3O_4/Ni and Co_3O_4@-NiMn-LDH/Ni are shown in the inset of Fig. 1b, e and h, respectively. It can be seen from Fig. 1b–d, the $Co_2(OH)_2CO_3$ precursor arrays are uniformly anchored on Ni foam, forming a fascicular and dense spinous structure. In addition, the SEM images of the pretreated Ni foam are displayed in Fig. S1. It is observed that the newly exposed surface of Ni foam is highly rough which is beneficial to the growth of $Co_2(OH)_2CO_3$ precursor arrays [37]. As displayed in Fig. 1e–g, the prepared sheet-like naostructure was assembled by the porous Co_3O_4 nanowires after the calcination in air, which is different from the fascicular and dense spinous structure of $Co_2(OH)_2CO_3$ precursors as displayed in Fig. 1c. Additionally, the porous Co_3O_4 nanowires are made up of plentiful nanoparticles as displayed in Fig. S2. These porous nanowires can not only utilize as skeleton support for growing the NiMn-LDHs nanosheets, but form an intricate transportation network to provide more paths for ions diffusion. It can be seen from Fig. 1h–j the NiMn-LDHs nanosheets are arrayed on the surface of porous Co_3O_4 nanowires to form a multi-layer structure. Moreover, the thickness of NiMn-LDHs was further confirmed by atomic force microscope (AFM) and the thickness was measured to be about 4 nm as shown in Fig. S3. From the SEM image as displayed in Fig. 1j, it also can be seen that the thickness of NiMn-LDHs is approximately 4 nm, which is accord with the result of AFM. The hybrid arrays provide large surface areas and enormous active sites, which can act a significant factor in enhancing the electrochemical performance. The cross-sectional SEM images (as displayed in Fig. S4) demonstrate that the NiMn-LDHs are uniformly anchored on the whole surface of the porous Co_3O_4 nanowires. Additionally, the SEM images of NiMn-LDH/Ni are displayed in Fig. S5.

Moreover, in order to further understand the evolution processes of the synthesized hierarchical and porous Co_3O_4@NiMn-LDH arrays, the synthesis of NiMn-LDHs was carried out with different reaction times and the SEM images of corresponding products are displayed in Fig. 2. The pure Co_3O_4 nanowires (Fig. 2a) with spinous structure can be served as the backbones for the growth of NiMn-LDHs arrays. NiMn-LDHs

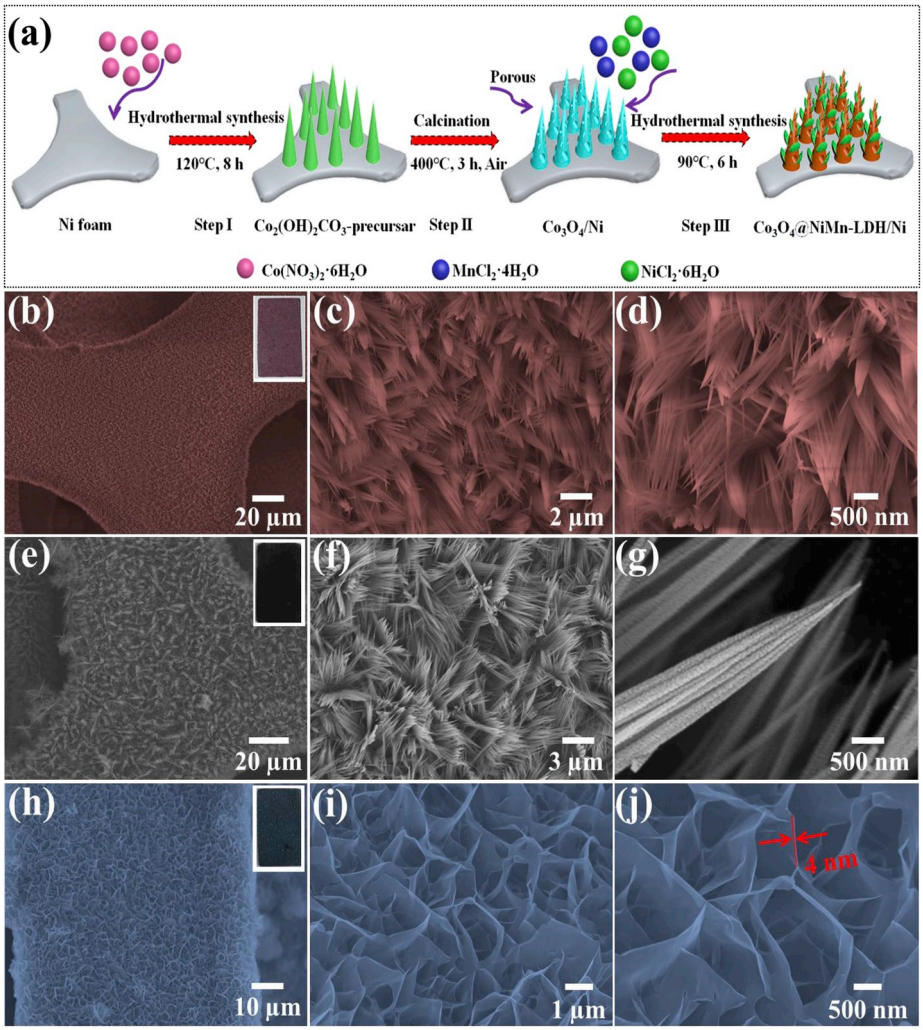

Fig. 1. (a) Schematic illustration for the step-wise preparation of Co_3O_4@NiMn-LDH arrays on Ni foam. (b–d) The SEM images of the $Co_2(OH)_2CO_3$ precursor arrays with different magnifications. (e–g) The SEM images of porous Co_3O_4 nanowires arrays with different magnifications. (h–j) The SEM images of Co_3O_4@NiMn-LDHs with different magnifications.

nanosheets were generated and fully covered on the surface of Co_3O_4 nanowires after 1 h reaction (Fig. 2b). Then the NiMn-LDHs nanosheets became dense and connected each other with the reaction time increasing to 2 h as displayed in Fig. 2c. After 4 h, the interconnected NiMn-LDHs nanosheets were further grown to become volume-expanded nanosheets as displayed in Fig. 2d. After 6 h reaction (Fig. 2e), the NiMn-LDHs nanosheets were expanded completely. After 8 h, the NiMn-LDHs nanosheets began to aggregate to form the spherical structures with uneven sizes (Fig. 2f). Additionally, the electrochemical performance of corresponding products from different reaction periods (Fig. S6) was further investigated by cyclic voltammetry (CV) and galvanostatic charge/discharge (GCD). As displayed in Fig. S6i, the Co_3O_4@NiMn-LDH/Ni obtained at 6 h exhibited the longest discharge time and the areal capacitance was measured to be 19.7 F cm^{-2}, which is much larger than those of other samples from 1 h (0.61 F cm^{-2}), 2 h (0.69 F cm^{-2}), 4 h (11.4 F cm^{-2}) and 8 h (11.1 F cm^{-2}) reactions, respectively. The multilayer structure of NiMn LDHs nanosheets obtained from 6 h reaction can not only expose enormous active sites for the redox reactions, but provide effective channels for electrolyte ion diffusion. For comparison, the weight ratios obtained from different reaction times between Co_3O_4 and NiMn materials are displayed in Table S1. It can be seen that the Co_3O_4@NiMn-LDH/Ni with optimized weight ratio of 1 : 2 for Co_3O_4: NiMn exhibits the superior capacitance than those with other different weight ratios.

To better understand the chemical composition of the as-fabricated porous Co_3O_4@NiMn-LDH/Ni, transmission electron microscopy (TEM), high resolution transmission electron microscopy (HRTEM), selected area electron diffraction (SAED) and energy dispersive X-ray spectroscopy (EDX) measurements were performed. Fig. 3a exhibits the TEM image of the porous Co_3O_4 nanowires. The nanowire composed of nanoparticles is highly porous, which is accord with the SEM images in Fig. 1g. The existed micropore structure provides more channels for ions shuttling and is beneficial to the intercalation of ions into the interior space of nanowires which further improves the reaction efficiency. From the HRTEM image of porous Co_3O_4 nanowires as displayed in Fig. 3b, the lattice fringes with spacings of 0.13, 0.17, 0.24 and 0.30 nm should be ascribed to the (440), (511), (311) and (220) facets of the cubic Co_3O_4, respectively. Moreover, the element mapping images of porous Co_3O_4 nanowires as displayed in Fig. S7, demonstrate that the Co and O elements are homogeneous existed in Co_3O_4 nanowires. Fig. 3d shows the well formation of thin NiMn-LDHs. Fig. 3e reveals the lattice spacing of 0.23 and 0.26 nm, which should be attributed to the (015) and (012) planes of NiMn-LDH phase, demonstrating the formation of NiMn-LDHs [38].

In addition, the SAED patterns reveal well-defined diffraction rings as displayed in Fig. 3c and f, demonstrating the polycrystalline structure of obtained porous Co_3O_4 nanowires and NiMn-LDHs, respectively. Moreover, the chemical composition of Co_3O_4@NiMn-LDH/Ni was studied by energy-dispersive X-ray spectroscopy (EDS). As displayed in Fig. 3g–i, the Co_3O_4@NiMn-LDH/Ni is consisted of Co, O, Ni and Mn elements, which are uniformly distributed. Moreover, the element mapping images of NiMn-LDHs are displayed in Fig. S8, which reveal the homogeneous distribution of Ni, O and Mn elements in NiMn-LDHs.

The phase composition and crystallinity of Ni foam, Co_3O_4/Ni and Co_3O_4@NiMn-LDH/Ni were analyzed by X-ray diffraction (XRD). Additionally, the detailed XRD spectra for NiMn-LDHs and $Co_2(OH)_2CO_3$ precursor/Ni are shown in Fig. S9. As displayed in Fig. 4a, all the as-obtained samples have the three characteristic peaks located at $2\theta = 44.50°$, 51.85° and 76.37°, which can be attributed to the (111), (200) and (220) planes of the cubic phase metallic nickel (JCPDS 04–0850), respectively. The Co_3O_4@NiMn-LDH/Ni shows diffraction peaks appeared at $2\theta = 31.27°$, 36.84°, 59.35° and 65.23°, which should attribute to the (220), (311), (511) and (440) planes of the cubic phase Co_3O_4 (JCPDS 42–1467), respectively. In addition, three weak diffraction peaks observed at $2\theta = 11.64°$, 34.43° and 38.72° can be indexed to the (003), (012) and (015) planes of NiMn-LDHs, respectively [39].

Furthermore, X-ray photoelectron spectroscopy (XPS) measurement was performed to analyze the elemental composition and chemical state of Co_3O_4@NiMn-LDH/Ni. The full survey scan XPS spectrum of Co_3O_4@NiMn-LDH/Ni is displayed in Fig. S10, from which the Co, O, Ni and Mn elements can be identified expressly. The spectrum of Co 2p is displayed in Fig. 4b, the peaks located at 780.5 eV and 795.8 eV should attribute to Co $2P_{3/2}$ (Co^{3+}) and Co $2P_{1/2}$ (Co^{2+}), respectively [40]. For O 1s spectrum displayed in Fig. 4c, the strong peak at 529.65 and 530.45 eV can be related to the O atoms in Co_3O_4 and hydroxyl group in NiMn-LDHs, respectively [41]. Similarly, as displayed in Fig. 4d, the peaks located at 854.45 eV and 872.15 eV can be attributed to Ni $2p_{3/2}$ and Ni $2p_{1/2}$, indicating the existence of Ni^{2+} [36,42]. The Mn 2p spectrum (Fig. 4e) is deconvoluted into two main peaks at 644.55 eV and 657.8 eV, which pertain to the characteristic peak of Mn $2p_{3/2}$ and Mn $2p_{1/2}$, respectively, demonstrating that the existence of Mn^{3+} in Co_3O_4@NiMn-LDH/Ni [43,44]. The Brunauer-Emmett-Teller (BET) measurement for the Co_3O_4@NiMn-LDH/Ni material has been carried out and the result is displayed in Fig. 4f. The specific surface area of Co_3O_4@NiMn-LDH/Ni was measured to be 310 $m^2 g^{-1}$, which was larger than those of Co_3O_4/Ni (28 $m^2 g^{-1}$) and NiMn-LDH/Ni (52 $m^2 g^{-1}$). This large surface area can provide enormous active sites for achieving an outstanding electrochemical performance. Meanwhile,

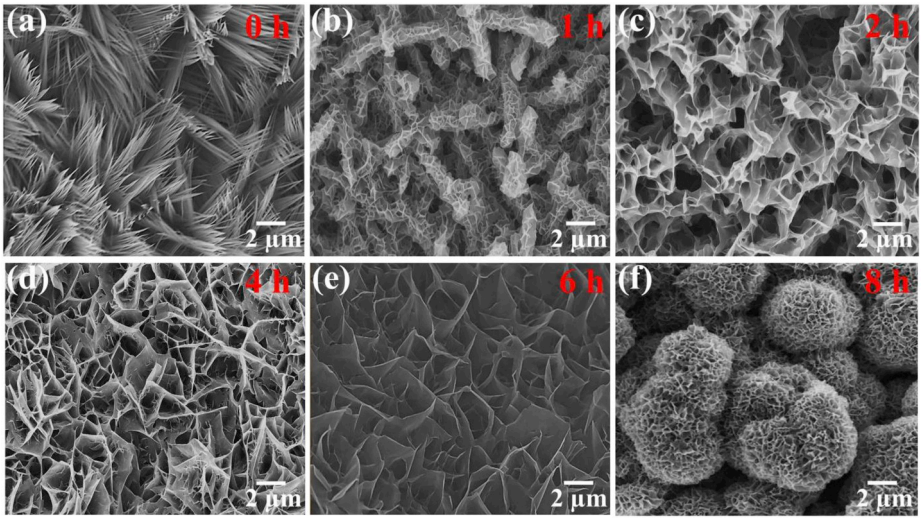

Fig. 2. SEM images of the samples obtained at different reaction times for NiMn-LDHs arrays: (a) 0 h, (b) 1 h, (c) 2 h, (d) 4 h, (e) 6 h and (f) 8 h, respectively.

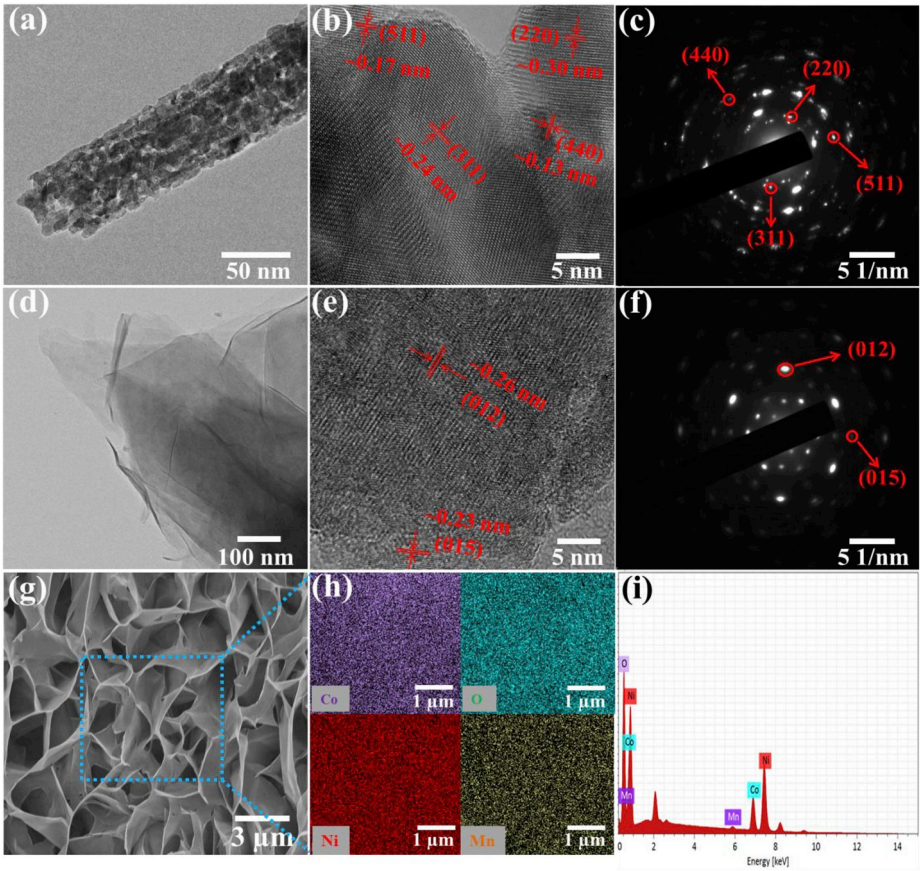

Fig. 3. (a) TEM image, (b) HRTEM image and (c) SAED image of porous Co_3O_4 nanowires. (d) TEM image, (e) HRTEM image and (f) SAED image of NiMn-LDHs. (g) Typical SEM image of Co_3O_4@NiMn-LDH/Ni and (h) the elemental mapping images for Co, O, Ni and Mn elements. (i) EDS spectrum for Co_3O_4@NiMn-LDH/Ni.

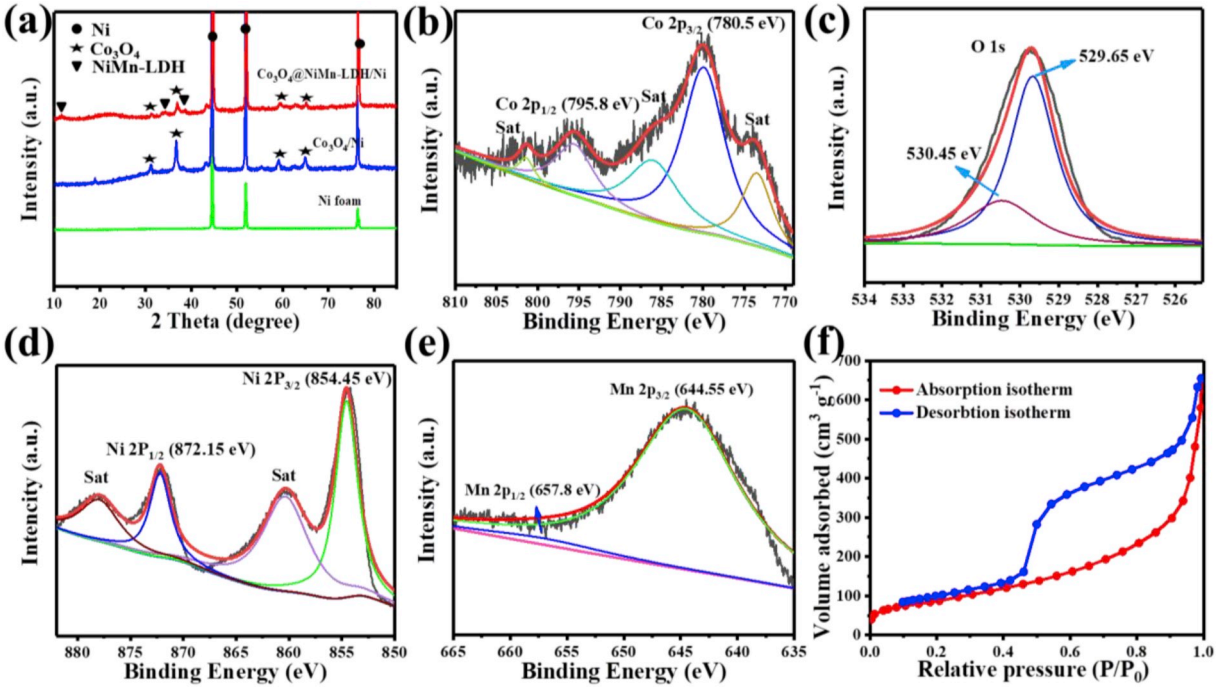

Fig. 4. (a) XRD patterns of the Ni foam, Co_3O_4/Ni and Co_3O_4@NiMn-LDH/Ni, respectively. Narrow scan spectra for Co 2p (b), O 1s (c), Ni 2p (d), and Mn 2p (e) of Co_3O_4@NiMn-LDH/Ni, respectively. (f) N_2 adsorption-desorption isotherm of Co_3O_4@NiMn-LDH/Ni.

the results of Brunauer-Emmett-Teller (BET) measurement tests for the Co_3O_4/Ni and NiMn-LDH/Ni are displayed in Fig. S11.

The electrochemical performances of Co_3O_4/Ni, NiMn-LDH/Ni and Co_3O_4@NiMn-LDH/Ni electrodes were performed in 6 M KOH electrolyte basing on a three-electrode system. The CV curves for Co_3O_4/Ni, NiMn-LDH/Ni and Co_3O_4@NiMn-LDH/Ni electrodes measured at a san rate of 10 mV s^{-1} are displayed in Fig. 5a. Compared with the mentioned electrode materials, Co_3O_4@NiMn-LDH/Ni revealed the highest current densities and the broadest voltage range, indicating the larger specific capacitance. As displayed in Fig. 5b, GCD curves of Co_3O_4/Ni, NiMn-LDH/Ni and Co_3O_4@NiMn-LDH/Ni electrodes were measured at a current density of 2 mA cm^{-2}. The discharge time of Co_3O_4@NiMn-LDH/Ni electrode was derived to be 4924 s, which was much longer than 327 s and 478 s derived from Co_3O_4/Ni, NiMn-LDH/Ni electrodes, respectively. Meanwhile, the areal capacitance of Co_3O_4@NiMn-LDH/Ni was calculated to be 19.7 F cm^{-2}, while the areal capacitance of other Co_3O_4/Ni and NiMn-LDH/Ni was calculated to be 1.305 and 1.913 F cm^{-2}, respectively. The Co_3O_4@NiMn-LDH/Ni electrode exhibits much better electrochemical properties than Co_3O_4/Ni and NiMn-LDH/Ni electrodes, which can be ascribed to the larger surface areas that offer more activated sites and transmission channels for ion/electron store and transfer.

Furthermore, the electrochemical performance of Co_3O_4@NiMn-LDH/Ni electrode was further investigated systematically with cyclic voltammetry (CV), galvanostatic charge/discharge (GCD) and electrical impedance spectroscopy (EIS) measurements. Fig. 5c exhibits the CV curves of Co_3O_4@NiMn-LDH/Ni electrode at different scan rates from 10 to 100 mV s^{-1} with the voltage window of 0–0.6 V. The shape of CV curves changes only slightly with the scan rate increasing, demonstrating the low equivalent resistance and well rate capability of the fabricated Co_3O_4@NiMn-LDH/Ni electrode [45]. In the alkaline electrolyte, the pseudocapacitance behavior can be described by the following reactions [46,47]:

$$Ni(OH)_2 + OH^- \rightleftharpoons NiOOH + H_2O + e^-$$

$$Mn(OH)_2 + OH^- \rightleftharpoons MnOOH + H_2O + e^-$$

$$MnOOH + OH^- \rightleftharpoons MnO_2 + H_2O + e^-$$

$$Co_3O_4 + OH^- + H_2O \rightleftharpoons 3CoOOH + e^-$$

$$CoOOH + OH^- \rightleftharpoons CoO_2 + H_2O + e^-$$

Fig. 5d exhibits a good linear relationship among the anodic or

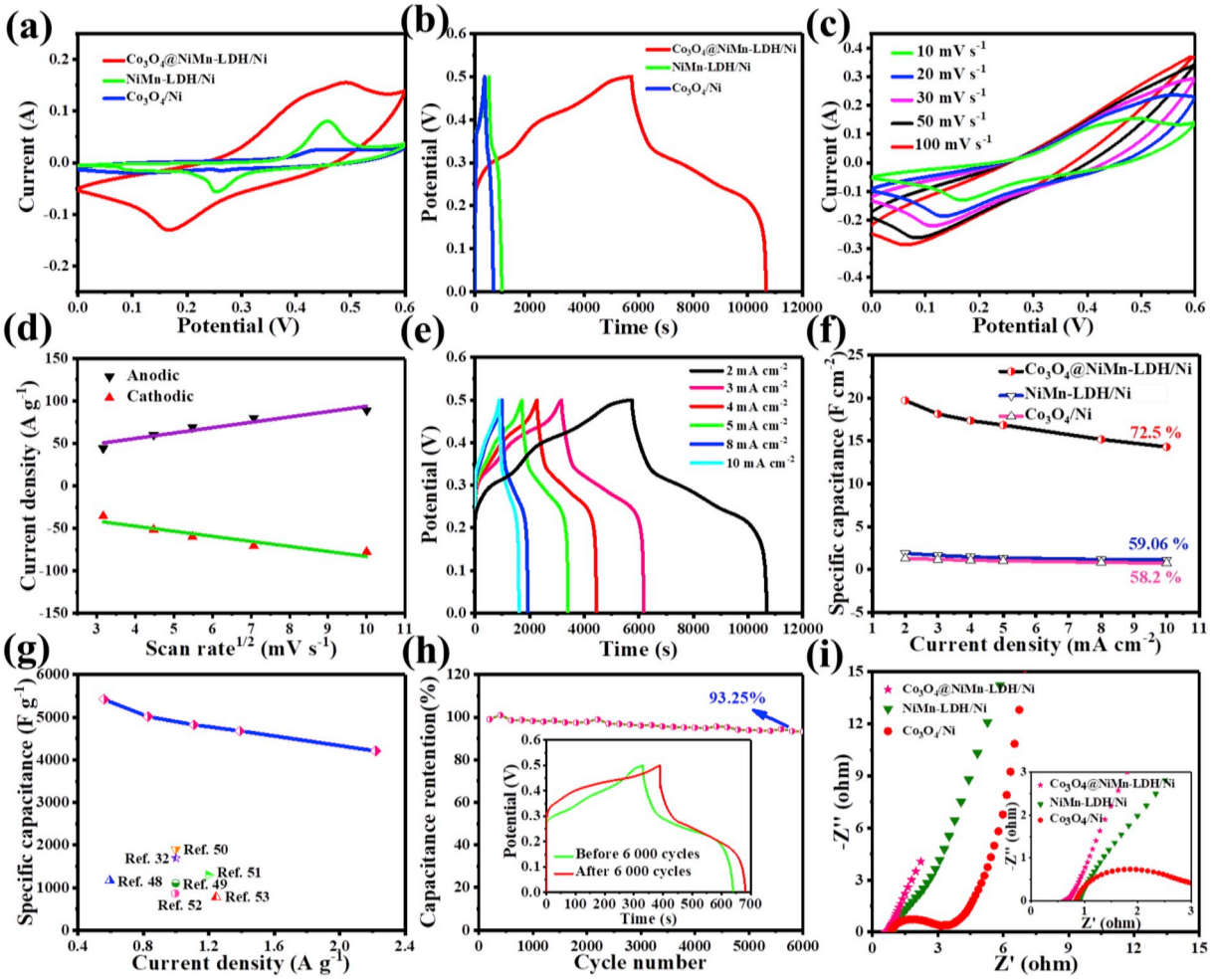

Fig. 5. Electrochemical performance measurements in three-electrode system. (a) CV curves of the Co_3O_4/Ni, NiMn-LDH/Ni and Co_3O_4@NiMn-LDH/Ni electrodes measured at a scan rate of 10 mV s^{-1}. (b) GCD curves of the Co_3O_4/Ni, NiMn-LDH/Ni and Co_3O_4@NiMn-LDH/Ni electrodes measured at a current density of 2 mA cm^{-2}. (c) CV curves of the Co_3O_4@NiMn-LDH/Ni electrode at different scan rates ranging from 10 to 100 mV s^{-1}. (d) The plots of anodic and cathodic peak current (A g^{-1}) against the scan rate (mV s^{-1}). (e) GCD curves of Co_3O_4@NiMn-LDH/Ni electrode at different current densities ranging from 2 to 10 mA cm^{-2}. (f) The linear relation of C_{sp} at different current densities. (g) A comparison of specific capacitance with those reported by the literatures. (h) Cycling performance of the Co_3O_4@NiMn-LDH/Ni electrode at 20 mA cm^{-2} (The inset shows the GCD curves of the Co_3O_4@NiMn-LDH/Ni electrode before and after 6000 cycles). (i) Nyquist curves of the Co_3O_4@NiMn-LDH/Ni, NiMn-LDH/Ni and Co_3O_4/Ni electrodes in the frequency range from 100 kHz to 0.01 Hz, respectively.

cathodic peak currents and the square root of scan rate from 10 mV s^{-1} to 100 mV s^{-1}, demonstrating the diffusion controlled process of OH^- [47]. The electrochemical reaction process was also verified from the triangle shape of the GCD curves of Co_3O_4@NiMn-LDH/Ni electrode at the different current densities from 2 to 10 mA cm^{-2} under the voltage window of 0–0.5 V as displayed in Fig. 5e. It is obvious that the discharge time decreased gradually with the increasing current density from 2 to 10 mA cm^{-2}. Moreover, the CV and GCD curves of Co_3O_4/Ni and NiMn-LDH/Ni electrodes are displayed in Fig. S12. The areal capacitances of Co_3O_4@NiMn-LDH/Ni were calculated to 19.7, 18.1, 17.3, 16.8, 15.1 and 14.2 F cm^{-2} at the current densities of 2, 3, 4, 5, 8 and 10 mA cm^{-2}, respectively. The relationships between specific capacitances and current densities of as-obtained samples are further displayed in Fig. 5f. It can be seen that the Co_3O_4@NiMn-LDH/Ni electrode exhibits the higher areal capacitances and rate capability of 72.5% than NiMn-LDH/Ni and Co_3O_4/Ni electrodes. The large specific capacitance value of Co_3O_4@NiMn-LDH/Ni can be attributed to the heterostructures of lamellar NiMn-LDHs supported by porous Co_3O_4 nanowires which explore enormous active sites for the redox reactions and provide effective channels for electrolyte ion diffusion. Fig. 5g shows that the prepared Co_3O_4@NiMn-LDH/Ni electrode possesses excellent specific capacitances of 5419.7 F g^{-1} at 0.56 A g^{-1}, which exhibits superb capacitance performance than recently reported electrode materials based on Co_3O_4 [32,48–53].

Cyclic stability, a significant evaluation index for supercapacitors, can be measured by repeated GCD measurements at a constant current density. As displayed in Fig. 5h, the Co_3O_4@NiMn-LDH/Ni electrode reveals an excellent stability and 93.25% of specific capacitance still maintains after 6000 cycles measurement at 20 mA cm^{-2}. The SEM images of the Co_3O_4@NiMn-LDH/Ni after 6000 cycles (Fig. S13) exhibited the partially collapsed multi-layered nanostructures. As displayed in the inset GCD curves in Fig. 5h, the decrease of discharge time after 6000 cycles should be attributed to the broken structures of NiMn-LDH nanosheets and the loss of active sites which affect the ion diffusion during charging-discharging process.

Electrochemical impedance spectroscopy (EIS) was utilized to analyze the internal resistances, charge transfer kinetics and ion diffusion process of electrode materials [54]. Fig. 5i clearly displays the EIS curves of NiMn-LDH/Ni, Co_3O_4/Ni and Co_3O_4@NiMn-LDH/Ni electrodes in the frequency range from 100 kHz to 0.01 Hz. It demonstrated that the Co_3O_4@NiMn-LDH/Ni possessed a lower charge-transfer resistance R_s of 0.62 Ω than those of Co_3O_4/Ni (0.85 Ω) and NiMn-LDH/Ni (0.92 Ω), indicating that the Co_3O_4@NiMn-LDH/Ni electrode material had the lower internal impedance and better conductivity [21]. Moreover, the straight line in the low frequency region is ascribed to Warburg impedance (Z_w) and the steep slope of the curves demonstrates the lower diffusive resistance of Co_3O_4@NiMn-LDH/Ni electrodes.

The excellent electrochemical properties of the prepared Co_3O_4@-NiMn-LDH/Ni can be ascribed to the following superiorities: Firstly, the porous Co_3O_4 nanowires directly grown on the conductive Ni foam maintains an efficient contact between the nanowires backbones and Ni substrate so as to provide an excellent conductivity to the whole electrode; Secondly, the porous Co_3O_4 nanowires are linked to NiMn-LDHs with strong adhesion, which can maintain the mechanical integrity of nanostructure and further improve the cycling stability. The mechanical stability of Co_3O_4@NiMn-LDH/Ni was tested in different ultrasonic frequencies from 50 Hz to 100 Hz for 80 s. As displayed in Fig. S14, the structure of NiMn-LDH nanosheets were only slightly changed, demonstrating the well mechanical stability of the Co_3O_4@NiMn-LDH/Ni. Moreover, the corresponding SEM images of Co_3O_4/Ni and NiMn-LDH/Ni samples from ultrasonications with different frequencies are displayed in Figs. S15 and S16, respectively. Thirdly, the ultra-thin NiMn-LDHs nanosheets are interconnected, which not only form a large area surface but also provide abundant active sites for electrochemical reactions during the charging-discharging process; Fourthly, the linked NiMn-LDHs nanosheets structure can not only provide effective channels for electrolyte ions diffusion, but also accelerate the transfer rate of electrolyte ions, further improving the electrochemical performance of active material. All of these advantages endow the Co_3O_4@NiMn-LDH/Ni with excellent capacitive performance.

To further evaluate the energy storage performance of Co_3O_4@-NiMn-LDH/Ni electrode for practical applications, an asymmetric supercapacitor (ASC) device (Co_3O_4@NiMn-LDH/Ni//AC) was successfully assembled by employing the Co_3O_4@NiMn-LDH/Ni composite as positive electrode and AC as negative electrode, respectively. Fig. 6a exhibits the individual CV curves of the positive and negative electrodes at the scan rate of 10 mV s^{-1} in a voltage range from 0 to 0.5 V and −1 to 0 V, respectively. Fig. 6b and c show the CV and GCD curves of the Co_3O_4@NiMn-LDH/Ni//AC ASC performed in different potential windows at 50 mV s^{-1} and 1 A g^{-1}, respectively. Obviously, the potential windows of Co_3O_4@NiMn-LDH/Ni//AC ASC can be enlarged to 1.5 V and the shapes of CV curves maintained almost the same in different potential windows. The high working voltage can decrease the number of devices needed to achieve the satisfied output potential, which performs a vital significance in practical applications. Meanwhile, all the GCD curves exhibit good symmetry and the shapes remained the same in different potential windows, which demonstrated the prominent capacitive performance. Fig. 6d exhibits the CV curves measured at different scan rates ranging from 10 to 100 mV s^{-1} in a potential window of 0–1.5 V. The GCD curves of Co_3O_4@NiMn-LDH/Ni//AC ASC device at different current densities from 0.5 to 8 A g^{-1} are displayed in Fig. 6e. The Co_3O_4@NiMn-LDH/Ni//AC ASC device exhibits a specific capacitance of 151.2 F g^{-1} at 0.5 A g^{-1} and maintains 76.06 F g^{-1} at 5 A g^{-1} as displayed in Fig. 6f, revealing its good rate capability.

The power density and energy density are important parameters to investigate the performance of an energy storage device. A Ragone plot of the Co_3O_4@NiMn-LDH/Ni//AC ASC is displayed in Fig. 6g. The Co_3O_4@NiMn-LDH/Ni//AC ASC device presented a high energy density of 47.15 Wh kg^{-1} at 376 W kg^{-1} and the energy density maintains 21.47 Wh kg^{-1} even at 6750.4 W kg^{-1}, which are comparable than some of the reported devices, such as carbon-coated Ni–Mn layered double hydroxide (LNC)//AC (37.7 Wh kg^{-1} at 378.15 W kg^{-1}) [55], NiO/NiMn-LDH//AC (27.8 Wh kg^{-1} at 401.3 W kg^{-1}) [56], NiMn-LDH/rGO//AC (22.5 Wh kg^{-1} at 1000 W kg^{-1}) [57], NiO/-Co_3O_4//AC (23.8 Wh kg^{-1} at 750 W kg^{-1}) [58], $CoFe_2O_4$@MnO_2//AC (37 Wh kg^{-1} at 470 W kg^{-1}) [59] and NiMn-LDH/PC-x//AC (37 Wh kg^{-1} at 225 W kg^{-1}) [60]. As displayed in Fig. 6h, the fabricated Co_3O_4@NiMn-LDH/Ni//AC ASC device presented a well stability and 85.65% of capacitance still maintained after 6000 cycles. Moreover, the Co_3O_4@NiMn-LDH/Ni//AC ASC device exhibited an outstanding coulombic efficiency which was measured to be about 98.21% after 6000 cycles. Additionally, the GCD curves have no obvious change (inset of Fig. 6h) in the cycles, which further demonstrate a good cycle life of the Co_3O_4@NiMn-LDH/Ni//AC ASC device [61]. Furthermore, a LED indicator can be lit up for 12 min by three Co_3O_4@NiMn-LDH/Ni//AC ASCs connected in series as displayed in Fig. 6i, evidencing the potential applications of the as-fabricated hierarchical and porous Co_3O_4@-NiMn-LDH/Ni in high-performance supercapacitors or energy storage systems.

4. Conclusion

In summary, the Co_3O_4@NiMn-LDH arrays anchored on Ni foam were successful prepared via the two-step hydrothermal reactions with a combination of annealing process. Owing to the heterostructure assembled by the porous Co_3O_4 nanowires and the layered structure of NiMn-LDHs, the obtained Co_3O_4@NiMn-LDH/Ni electrode reveals a high specific capacitance of 19.7 F cm^{-2} at 2 mA cm^{-2} (5419.7 F g^{-1} at 0.56 A g^{-1}) and an outstanding cycling stability (93.25% capacitance maintained after 6000 cycles). Furthermore, the self-assembled asymmetric supercapacitor exhibits a high energy density of 47.15 Wh kg^{-1} at 376 W kg^{-1} and a well cycling stability (85.65% capacitance maintained

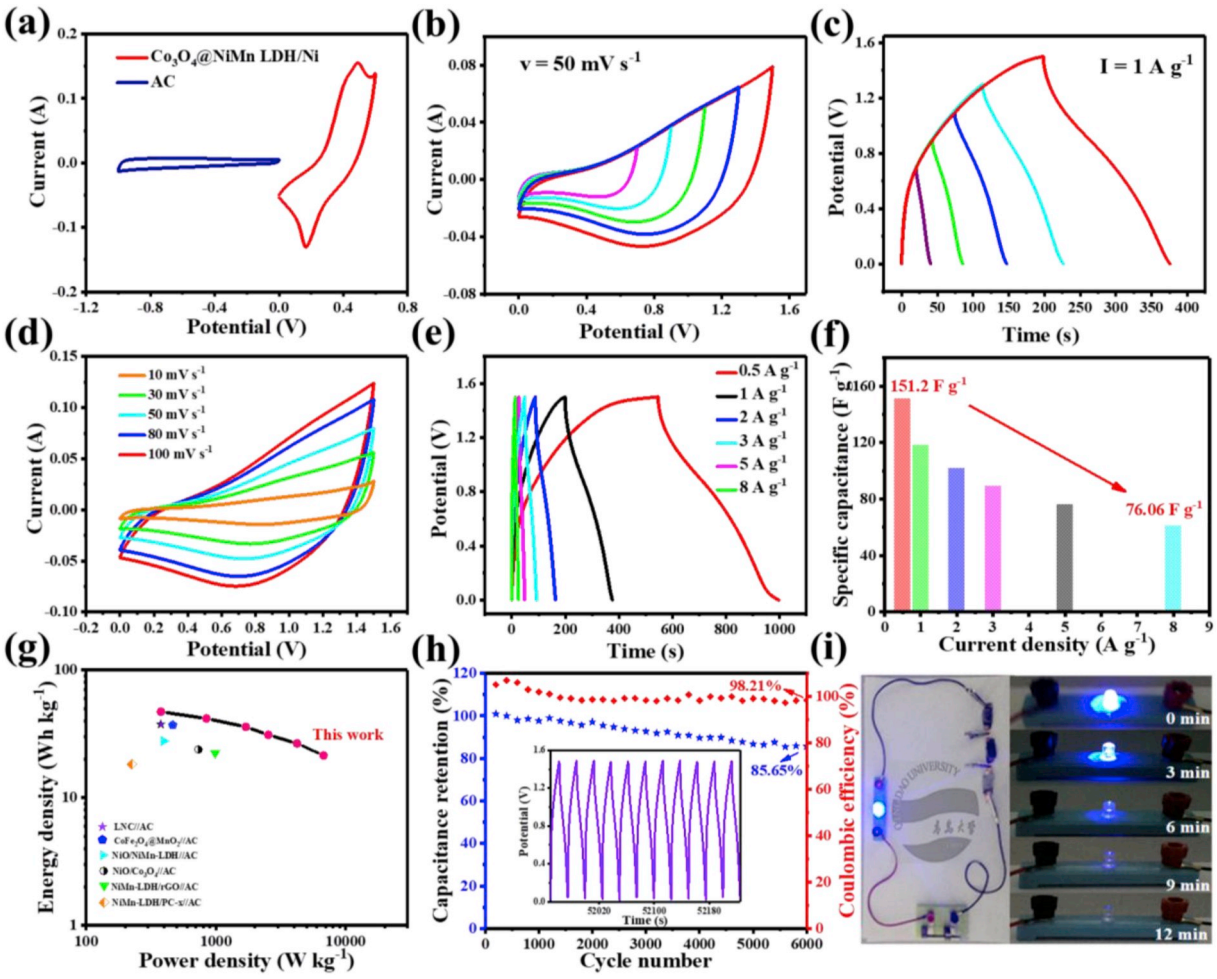

Fig. 6. (a) CV curves of AC and Co_3O_4@NiMn-LDH/Ni electrodes measured at the scan rate of 10 mV s^{-1} in a three-electrode system. (b) CV curves of Co_3O_4@NiMn-LDH/Ni//AC ASC measured at different potential windows at 50 mV s^{-1}. (c) GCD curves of Co_3O_4@NiMn-LDH/Ni//AC ASC measured at different potential windows at 1 A g^{-1}. (d) CV curves of Co_3O_4@NiMn-LDH/Ni//AC ASC at different scan rates. (e) GCD curves of Co_3O_4@NiMn-LDH/Ni//AC ASC at different current densities. (f) The specific capacitance of the ASC device at different current densities. (g) Ragone plot of Co_3O_4@NiMn-LDH/Ni electrode. (h) Cycling performance of the ASC device during 6000 cycles at a current density of 5 A g^{-1}. (i) The brightness intensity of LED indicator lit up by three all-solid-state ASCs connected in series for various time periods.

after 6000 cycles). Most importantly, the capability to light up a LED by three ASCs connected in series reveals that the synthesized Co_3O_4@-NiMn-LDH/Ni electrode material possesses great potential for practical applications. Therefore, it can be envisioned that the novel Co_3O_4@-NiMn-LDH/Ni electrode should have promising applications in energy storage devices and nanotechnology.

Acknowledgments

This work was supported by Qingdao Innovation Leading Expert Program, Taishan Scholars Program, National Natural Science Foundation of China (21805124), and Natural Science Foundation of Shandong Province (ZR2018BEM020).

Appendix A. Supplementary data

Supplementary data to this article can be found online at https://doi.org/10.1016/j.jpowsour.2019.227123.

References

[1] Y. Hu, Y. Zhang, C. Xu, L. Lin, R.L. Snyder, Z.L. Wang, Self-Powered system with wireless data transmission, Nano Lett. 6 (2011) 2572–2577.
[2] N.T. Suen, S.F. Hung, Q. Quan, N. Zhang, Y.J. Xu, H.M. Chen, Electrocatalysis for the oxygen evolution reaction: recent development and future perspectives, Chem. Soc. Rev. 2 (2017) 337.
[3] S.H. Lee, K.J. Chang, G.T. Hwang, K.J. Lee, Self-powered flexible inorganic electronic system, Nano Energy 14 (2015) 111–125.
[4] T. Zhai, L. Wan, S. Sun, Q. Chen, J. Sun, Q. Xia, H. Xia, Phosphate ion functionalized Co_3O_4 ultrathin nanosheets with greatly improved surface reactivity for high performance pseudocapacitors, Adv. Mater. 7 (2017) 1604167.
[5] J. Yan, Q. Wang, T. Wei, Z. Fan, Recent advances in design and fabrication of electrochemical supercapacitors with high energy densities, Adv. Energy Mater. 4 (2014) 1300816.
[6] M. Salanne, B. Rotenberg, K. Naoi, K. Kaneko, P.L. Taberna, C.P. Grey, B. Dunn, P. Simon, Efficient storage mechanisms for building better supercapacitors, Nat. Energy. 6 (2016) 16070.
[7] H.S. Chavan, B. Hou, A.T.A. Ahmed, Y. Jo, S. Cho, J. Kim, S.M. Pawar, S. Cha, A. I. Inamdar, H. Im, H. Kim, Nanoflake $NiMoO_4$ based smart supercapacitor for intelligent power balance monitoring, Sol. Energy Mater. Sol. Cells 185 (2018) 166–173.
[8] A.I. Inamdar, J. Kim, Y. Jo, H. Woo, S. Cho, S.M. Pawar, S. Lee, J.L. Gunjakar, Y. Cho, B. Hou, S. Cha, J. Kwak, Y. Park, H. Kim, H. Im, Highly efficient electro-optically tunable smart-supercapacitors using an oxygen-excess nanograin tungsten oxide thin film, Sol. Energy Mater. Sol. Cells 166 (2017) 78–85.
[9] P. Chang, K. Matsumura, J. Zhang, J. Qi, C. Wang, T. Kinumoto, T. Tsumura, M. Chen, M. Toyoda, 2D porous carbon nanosheets constructed of few-layer graphene sheets by "medium-up" strategy for ultrahigh power-output EDLCs, J. Mater. Chem. A. 22 (2018) 10331–10339.
[10] A.G. Kannan, A. Samuthirapandian, D.W. Kim, Electric double layer capacitors employing nitrogen and sulfur co-doped, hierarchically porous graphene electrodes with synergistically enhanced performance, J. Power Sources 337 (2017) 65–72.

[11] L. Jiang, L. Sheng, X. Chen, T. Wei, Z. Fan, Construction of nitrogen-doped porous carbon buildings using interconnected ultra-small carbon nanosheets for ultra-high rate supercapacitors, J. Mater. Chem. A. 29 (2016) 11388–11396.

[12] I. Yang, D. Kwon, M.S. Kim, C.J. Ji, A comparative study of activated carbon aerogel and commercial activated carbons as electrode materials for organic electric double-layer capacitors, Carbon 132 (2018) 503–511.

[13] P. Hao, J. Tian, Y. Sang, C.C. Tuan, G. Cui, X. Shi, C. Wong, B. Tang, H. Liu, 1D Ni-Co oxide and sulfide nanoarray/carbon aerogel hybrid nanostructures for asymmetric supercapacitors with high energy density and excellent cycling stability, Nanoscale 36 (2016) 16292–16301.

[14] P. Hao, Z. Zhao, Y. Leng, J. Tian, Y. Sang, R.I. Boughton, C. Wong, H. Liu, B. Yang, Graphene-based nitrogen self-doped hierarchical porous carbon aerogels derived from chitosan for high performance supercapacitors, Nano Energy 15 (2015) 9–23.

[15] Y. Wang, H. Dou, B. Ding, J. Wang, Z. Chang, Y. Xu, X. Hao, Nanospace-confined synthesis of oriented porous carbon nanosheets for high-performance electrical double layer capacitors, J. Mater. Chem. A. 43 (2016) 16879–16885.

[16] R.X.,T.H., Y.Q., Nanostructured metal sulfides for energy storage, Nanoscale 17 (2014) 9889–9924.

[17] C. Yuan, L. Yang, L. Hou, L. Shen, X. Zhang, X.W. Lou, Growth of ultrathin mesoporous Co_3O_4 nanosheet arrays on Ni foam for high-performance electrochemical capacitors, Energy Environ. Sci. 7 (2012) 7883–7887.

[18] R.B. Rakhi, W. Chen, D. Cha, H.N. Alshareef, Substrate dependent self-organization of mesoporous cobalt oxide nanowires with remarkable pseudocapacitance, Nano Lett. 5 (2012) 2559–2567.

[19] P. Yang, W. Mai, Flexible solid-state electrochemical supercapacitors, Nano Energy 6 (2014) 274–290.

[20] M. Zhang, H. Fan, N. Zhao, H. Peng, X. Ren, W. Wang, H. Li, G. Chen, Y. Zhu, X. Jiang, 3D hierarchical $CoWO_4/Co_3O_4$ nanowire arrays for asymmetric supercapacitors with high energy density, Chem. Eng. J. 347 (2018) 291–300.

[21] Y. Lu, L. Li, D. Chen, G. Shen, Nanowire-assembled Co_3O_4@$NiCo_2O_4$ architectures for high performance all-solid-state asymmetric supercapacitors, J. Mater. Chem. A. 47 (2017) 24981–24988.

[22] J.J. Zhou, Q. Li, C. Chen, Y.L. Li, K. Tao, L. Han, Co_3O_4@CoNi-LDH core/shell nanosheet arrays for high-performance battery-type supercapacitors, Chem. Eng. J. 350 (2018) 551–558.

[23] L. Xing, Y. Dong, F. Hu, X. Wu, A. Umar, Co_3O_4 nanowire@NiO nanosheet arrays for high performance asymmetric supercapacitors, Dalton Trans. 16 (2018) 5687–5694.

[24] Y. Liu, X. Cao, D. Jiang, D. Jia, J. Liu, Hierarchical CuO nanorod arrays in situ generated on three-dimensional copper foam via cyclic voltammetry oxidization for high-performance supercapacitors, J. Mater. Chem. A. 22 (2018) 10474–10483.

[25] P. Hao, Z. Zhao, L. Li, C.C. Tuan, H. Li, Y. Sang, H. Jiang, C. Wong, H. Liu, The hybrid nanostructure of $MnCo_2O_{4.5}$ nanoneedle/carbon aerogel for symmetric supercapacitors with high energy density, Nanoscale 7 (2015) 14401–14412.

[26] P. Hao, Z. Zhao, J. Tian, H. Li, Y. Sang, G. Yu, H. Cai, H. Liu, C. Wong, A. Umar, Hierarchical porous carbon aerogel derived from bagasse for high performance supercapacitor electrode, Nanoscale 6 (2014) 12120–12129.

[27] M. Zhao, Q. Zhao, B. Li, H. Xue, H. Pang, C. Chen, Recent progress in layered double hydroxide based materials for electrochemical capacitors: design, synthesis and performance, Nanoscale 40 (2017) 15206–15225.

[28] P.F. Liu, J.J. Zhou, G.C. Li, M.K. Wu, K. Tao, F.Y. Yi, W.N. Zhao, L. Han, A hierarchical NiO/NiMn-layered double hydroxide nanosheet array on Ni foam for high performance supercapacitors, Dalton Trans. 23 (2017) 7388–7391.

[29] M. Yu, W. Wang, C. Li, T. Zhai, X. Lu, Y. Tong, Scalable self-growth of Ni@NiO core-shell electrode with ultrahigh capacitance and super-long cyclic stability for supercapacitors, NPG Asia Mater. 9 (2014) e129.

[30] Zhigang Zhao, Fengxia Geng, A. Jinbo Bai, Huiming Cheng, Facile and controlled synthesis of 3D nanorods-based urchinlike and nanosheets-based flowerlike cobalt basic salt nanostructures, J. Phys. Chem. C 10 (2007) 3848–3852.

[31] X. Xia, J. Tu, Y. Zhang, Y. Mai, X. Wang, C. Gu, X. Zhao, Freestanding Co_3O_4 nanowire array for high performance supercapacitors, RSC Adv. 5 (2012) 1835–1841.

[32] D. Kong, J. Luo, Y. Wang, W. Ren, T. Yu, Y. Luo, Y. Yang, C. Cheng, Three dimensional Co_3O_4@MnO_2 hierarchical nanoneedle arrays: morphology control and electrochemical energy storage, Adv. Funct. Mater. 24 (2014) 3815–3826.

[33] B. Zhao, L. Zhang, Q. Zhang, D. Chen, Y. Cheng, X. Deng, Y. Chen, R. Murphy, X. Xiong, B. Song, Rational design of nickel hydroxide-based nanocrystals on graphene for ultrafast energy storage, Adv. Energy Mater. 8 (2017) 1702247.

[34] J.H. Kim, D. Bhattacharjya, J.S. Yu, Synthesis of hollow TiO_2@N-doped carbon with enhanced electrochemical capacitance by an in situ hydrothermal process using hexamethylenetetramine, J. Mater. Chem. A. 29 (2014) 11472–11479.

[35] S. Tajik, D.P. Dubal, P. Gomez-Romero, A. Yadegari, A. Rashidi, B. Nasernejad, Inamuddin, A.M. Asiri, Nanostructured mixed transition metal oxides for high performance asymmetric supercapacitors: facile synthetic strategy, Int. J. Hydrogen Energy 42 (2017) 12384–12395.

[36] J. Lin, H. Jia, H. Liang, S. Chen, Y. Cai, J. Qi, C. Qu, J. Cao, W. Fei, J. Feng, Hierarchical $CuCo_2S_4$@NiMn-layered double hydroxide core-shell hybrid arrays as electrodes for supercapacitors, Chem. Eng. J. 336 (2018) 562–569.

[37] Q. Chen, J. Li, C. Liao, G. Hu, Y. Fu, O.K. Asare, S. Shi, Z. Liu, L. Zhou, L. Mai, Ni foam supported NiO nanosheets as high-performance free-standing electrodes for hybrid supercapacitors and Ni-Zn batteries, J. Mater. Chem. A. 40 (2018) 19488–19494.

[38] W. Guo, C. Yu, S. Li, J. Yang, Z. Liu, C. Zhao, H. Huang, M. Zhang, X. Han, Y. Niu, High-stacking-density, superior-roughness LDH bridged with vertically aligned graphene for high-performance asymmetric supercapacitors, Small 37 (2017) 1701288.

[39] J. Zhao, J. Chen, S. Xu, M. Shao, Q. Zhang, F. Wei, J. Ma, M. Wei, D.G. Evans, D. Xue, Flexible electronics: hierarchical NiMn layered double hydroxide/carbon nanotubes architecture with superb energy density for flexible supercapacitors, Adv. Funct. Mater. 20 (2014) 2938–2946 (Adv. Funct. Mater. 20/2014).

[40] H. Du, C. Wang, J. Lv, Controllable morphologies of Co_3O_4@MnO_2 core-shell structure grown on nickel foam and their supercapacitor behavior, Solid State Commun. 277 (2018) 19–24.

[41] J. Dupin, D. Gonbeau, P. Vinatier, A. Levasseur, Systematic XPS studies of metal oxides, hydroxides and peroxides, Phys. Chem. Chem. Phys. 6 (2017) 1319–1324.

[42] P.C. Chen, G. Shen, Y. Shi, H. Chen, C. Zhou, Preparation and characterization of flexible asymmetric supercapacitors based on transition-metal-oxide nanowire/single-walled carbon nanotube hybrid thin-film electrodes, ACS Nano 8 (2010) 4403.

[43] J. Sun, W. Li, B. Zhang, G. Li, L. Jiang, Z. Chen, R. Zou, J. Hu, 3D core/shell hierarchies of MnOOH ultrathin nanosheets grown on NiO nanosheet arrays for high-performance supercapacitors, Nano Energy 1 (2014) 56–64.

[44] H. Wan, L. Jia, Y. Ruan, L. Lin, P. Lu, J. Xiao, M. Ling, J. Jiang, Hierarchical configuration of $NiCo_2S_4$ nanotube@Ni-Mn layered double hydroxide arrays/three-dimensional graphene sponge as electrode materials for high-capacitance supercapacitors, ACS Appl. Mater. Interfaces 29 (2015) 15840.

[45] X. Wang, C. Yan, A. Sumboja, P.S. Lee, High performance porous nickel cobalt oxide nanowires for asymmetric supercapacitor, Nano Energy 1 (2014) 119–126.

[46] A.L. Yan, X.C. Wang, J.P. Cheng, Research progress of NiMn layered double hydroxides for supercapacitors: a review, Nanomaterials 10 (2018) 747.

[47] O. Moradlou, H. Ansarinejad, M. Hosseinzadeh, H. Kazemi, High-performance solid state asymmetric supercapacitor based on electrochemically decorated 3D network-like Co_3O_4 architecture on NiO nanoworms, J. Alloy. Comp. 755 (2018) 231–241.

[48] M. Li, Y. Wang, H. Yang, P.K. Chu, Hierarchical $CoMoO_4$@Co_3O_4 nanocomposites on an ordered macro-porous electrode plate as a multi-dimensional electrode in high-performance supercapacitors, J. Mater. Chem. A. 33 (2017) 17312–17324.

[49] X. Li, Z. Yang, W. Qi, Y. Li, Y. Wu, S. Zhou, S. Huang, J. Wei, H. Li, P. Yao, Binder-free Co_3O_4@NiCoAl-layered double hydroxide core-shell hybrid architectural nanowire arrays with enhanced electrochemical performance, Appl. Surf. Sci. 363 (2016) 381–388.

[50] S. Zhou, C. Hao, J. Wang, X. Wang, H. Gao, Metal-organic framework templated synthesis of porous $NiCo_2O_4/ZnCo_2O_4/Co_3O_4$ hollow polyhedral nanocages and their enhanced pseudocapacitive properties, Chem. Eng. J. 351 (2018) 74–84.

[51] X. Bai, Q. Liu, J. Liu, H. Zhang, Z. Li, X. Jing, P. Liu, J. Wang, R. Li, Hierarchical Co_3O_4@$Ni(OH)_2$ core-shell nanosheet arrays for isolated all-solid state supercapacitor electrodes with superior electrochemical performance, Chem. Eng. J. 315 (2017) 35–45.

[52] D. Cai, H. Huang, D. Wang, B. Liu, L. Wang, Y. Liu, Q. Li, T. Wang, High-performance supercapacitor electrode based on the unique ZnO@Co_3O_4 core/shell heterostructures on nickel foam, ACS Appl. Mater. Interfaces 18 (2014) 15905–15912.

[53] H.L. Zhu, Y.Q. Zheng, Mesoporous Co_3O_4 anchored on the graphitic carbon nitride for enhanced performance supercapacitor, Electrochim. Acta 265 (2018) 372–378.

[54] Y. Li, L. Cao, L. Qiao, M. Zhou, Y. Yang, P. Xiao, Y. Zhang, Ni-Co sulfide nanowires on nickel foam with ultrahigh capacitance for asymmetric supercapacitors, J. Mater. Chem. A. 18 (2014) 6540–6548.

[55] H. Chen, Y. Ai, F. Liu, X. Chang, Y. Xue, Q. Huang, C. Wang, H. Lin, S. Han, Carbon-coated hierarchical Ni-Mn layered double hydroxide nanoarrays on Ni foam for flexible high-capacitance supercapacitors, Electrochim. Acta 213 (2016) 55–65.

[56] L PF, Z JJ, L GC, W MK, T.K, Y. FY, Z. WN, H.L, A hierarchical NiO/NiMn-layered double hydroxide nanosheet array on Ni foam for high performance supercapacitors, Dalton Trans. 23 (2017) 7388–7391.

[57] M. Padmini, S.K. Kiran, N. Lakshminarasimhan, M. Sathish, P. Elumalai, High-performance solid-state hybrid energy-storage device consisting of reduced graphene-oxide anchored with NiMn-layered double hydroxide, Electrochim. Acta 236 (2017) 359–370.

[58] J. Qiu, Z. Bai, E. Dai, S. Liu, Y. Liu, NiO/Co_3O_4 nanoheterostructure derived from nickelocene filled ZIF-67 for supercapacitors, J. Alloy. Comp. 763 (2018) 966–974.

[59] H. Gao, S. Cao, Y. Cao, Hierarchical core-shell nanosheet arrays with MnO_2 grown on mesoporous $CoFe_2O_4$ support for high-performance asymmetric supercapacitors, Electrochim. Acta 240 (2017) 31–42.

[60] M. Yu, R. Liu, J. Liu, S. Li, Y. Ma, Polyhedral-like NiMn-layered double hydroxide/porous carbon as electrode for enhanced electrochemical performance supercapacitors, Small 44 (2017) 1702616.

[61] W. Huang, A. Zhang, H. Liang, R. Liu, J. Cai, L. Cui, J. Liu, Novel fabrication of hollow and spinous $NiCo_2S_4$ nanotubes templated by natural silk for all-solid-state asymmetric supercapacitors, J. Colloid Interface Sci. 549 (2019) 140–149.